Astronomy & Astrophysics manuscript no. paper7 February 9, 2005
(DOI: will be inserted by hand later)

Spectroscopic signatures of the M 1.0 flare on October 22, 2002

G. Del Zanna[1⋆], A. Berlicki[2,3], H. E. Mason[4], and B. Schmieder[2,5]

[1] MSSL, University College London Holmbury St. Mary Dorking UK RH5 6NT
[2] Observatoire de Paris, Section de Meudon, LESIA, F-92195 Meudon Principal Cedex, France
[3] Astronomical Institute of the Wrocław University, ul. Kopernika 11, 51-622 Wrocław, Poland
[4] Department of Applied Mathematics and Theoretical Physics, University of Cambridge, Cambridge UK CB3 0WA
[5] Institute of Theoretical Astrophysics, University of Oslo, Blindern, N-0315 Oslo, Norway

February 9, 2005

Abstract. In this paper we present a further study of the M1 class flare observed on 22nd October 2002. We focus on the SOHO Coronal Diagnostic Spectrometer (CDS) spectral observations and the ground-based (VTT/MSDP) observations performed during a multi-wavelength campaign with TRACE. Strong blue-shifts are observed in the CDS coronal and flare lines during the impulsive phase of this flare. From a careful wavelength calibration we deduce upflows of 140 km/s for the Fe XIX emission. We relate these to upflows deduced from the Hα features seen with the VTT/MSDP. The Hα emission is analysed using non-LTE models. These results contrast with other publications which show downflows in Hα emission correlated with upflows in high temperature emission. We interpret our results as due to 'gentle evaporation'. In the upflow regions we measure electron densities $\simeq 10^{11}$ cm^{-3} in transition region lines. SOHO/MDI magnetograms show changes during the flare, indicative of flux cancellation. We discuss the importance of spectral observations in relation to our understanding of the development of flares. We consider the complexity and limitations of current spectroscopic observations and look towards future solar missions, such as Solar-B.

Key words. Sun: corona – Techniques: spectroscopic – Line: profiles

1. Introduction

An important aspect of flare evolution is the presence of flows. These are characterised by asymmetrical profiles of spectral lines. These asymmetries or line shifts (particularly in the blue wing) have been observed both in X-ray and in chromospheric lines. They are thought to be caused predominantly by vertical mass motions in flaring layers of the solar atmosphere. It is now widely accepted that during flares the chromospheric plasma is evaporated into the corona providing material for the so-called post-flare loops (Antiochos & Sturrock 1978).

The broadening and blue-shifting of spectral lines for high temperature emission during the initial phase of solar flares has been extensively studied in the X-ray wavelength range using data from SOLFLEX (cf. Doschek et al. 1979), the Solar Maximum Mission's (SMM's) X-ray polychromator (XRP) Bent Crystal Spectrometer (BCS) (cf Antonucci et al. 1982) and the BCS on YOHKOH (see, e.g., Bentley et al. 1994). Plasma velocities deduced from Doppler-shift analysis were of the order of a few hundreds km s^{-1}. This blueshifted emission was interpreted as evidence for chromospheric evaporation. However, these BCSs had no spatial resolution, so it was not possible to locate the source of the blueshifted X-ray emission, or to spatially separate this from any stationary components. A further complexity in the interpretation of BCS spectra was due to the superposition (at different wavelengths) of stationary components originating from different locations. In general asymetric line profiles were observed, rather than totally shifted lines. Without spatial resolution in the BCS X-ray observations, any weak blueshifted X-ray emission would swiftly be swamped by the strong stationary emission from the flare X-ray loops. In a recent paper, Warren & Doschek (2005) interpret these blue-shifted asymetries as a succession of independently heated threads within flare loop structures. To progress further, it is essential to spatially locate the high temperature blue shifted emission in relation to the flare loops and structures. This can only be achieved with a spectrometer which also has good spatial resolution. Observations of this kind are extremely rare.

Send offprint requests to: G. Del Zanna
(G.Del-Zanna@damtp.cam.ac.uk)
⋆ Previous address: DAMTP, University of Cambridge

The SMM XRP Flat Crystal Spectrometer (FCS) had a limited spatial resolution (14″). Zarro et al. (1988) reported spatially confined Mg XI blue-shifted emission during the impulsive phase of a small flare. The Fe XXI line at 1354.1 Å emitted at about 10^7 K, was studied with the SMM Ultraviolet Spectrometer and Polarimeter (UVSP) instrument (with spatial resolution down to 3″) . Mason et al. (1986) deduced upward flows in Fe XXI emitting plasma in excess of 200 km/s. Their observations supported the hypothesis of chromospheric evaporation in the 'footpoint region' of what subsequently became soft X-ray emitting loops. Schmieder et al. (1990) studied the evaporation in the transition region during the gradual phase of solar flares. From SMM/UVSP CIV emission and HXIS data, they found both upflows of 4-12 km s^{-1} and downflows of about 10 km s^{-1}. They interpreted the results in terms of the chromospheric ablation model proposed by Forbes et al. (1989).

The Coronal Diagnostic Spectrometer (CDS) instrument on SOHO has the capability to simultaneously obtain spatial and spectral information for emission over a wide range of plasma temperatures. One of the hottest lines recorded with CDS is the Fe XIX flare line at 592.2 Å. This is formed at a temperature around 8×10^6 K. Using CDS, it is possible to locate the source of high temperature blue-shifted emission seen during a solar flare. Czaykowska et al. (1999) reported SOHO/CDS observations of blue-shifts in Fe XVI (3×10^6 K) and Fe XIX (8×10^6 K) lines. These observations were however performed more than one hour after the maximum of a two-ribbon M6.8 flare. The blue-shifts appeared to be located at the outer edges of the flare ribbons.

Spatially-resolved spectral information from CDS were reported by Del Zanna et al. (2002a) covering the entire evolution of a small flare. Long-lasting (over an hour) blue-shifts of 30 km/s in coronal lines (Mg X, Si XII, emitted at 1-2 MK) were located at the footpoints of a small loop system. These could be interpreted as indirect evidence of chromospheric evaporation. The hotter Fe XIX emission also showed some interesting properties, including a pre-flare enhancement along the loop structure (Gibson et al. 2002). A long-term campaign of SOHO/CDS observations over 2001-2004 has provided evidence that similar features are common in C-class flares (see Del Zanna et al. 2002b).

Recently, Teriaca et al. (2003) published CDS and ground-based observations of an eruptive C2 flare. The main findings were quasi-simultaneous and co-spatial measurements of upflows in the flare line (Fe XIX) and downflows in the chromosphere, as seen in the He I 10830 Å line. Brosius & Phillips (2004) presented CDS observations of a larger M6 flare. These authors kept the position of the CDS slit fixed, thus sacrifying spatial coverage in favour of a high (10s) time resolution. They used TRACE observations to track the evolution of the flare. Their main results were measurements of upflows ($\simeq$60 km/s) in flare lines and downflows ($\simeq$40 km/s) in cooler transition region lines during the impulsive phase. The X-ray emission appeared $\simeq$1m after the start of the impulsive intensity rise in the cooler lines. They concluded that their observations were consistent with non-thermal particles transferring most of the energy into the chromosphere and creating these oppositely-directed flows.

The "explosive" evaporation seen in the emission from high temperature flare plasma is thought to be driven by non-thermal electrons accelerated during the primary energy release (Antonucci et al. 1984) and may occur when the heating rate due to collisions of non-thermal electrons with the ambient plasma in upper layers of the chromosphere exceeds the chromospheric radiative losses (Fisher 1987). This occurs when the temperature of the heated region is above 2×10^5 K and thus this kind of evaporation cannot be seen in chromospheric spectral lines which are formed in a cooler plasma.

If a region of the chromosphere heated by non-thermal electrons is thick enough, then the rapid temperature increase produces an enhanced pressure in the heated region. This overpressure, besides the evaporation, also drives downward-moving cool and dense *chromospheric condensations* (Fisher et al. 1985a) which seem to be responsible for red-shifts of the Hα line profiles reported by many authors (Svestka 1976, Ichimoto & Kurokawa 1984). Fisher et al. (1985c) modelled the hydrodynamic and radiative response of the atmosphere to short impulsive injections of non-thermal electron beams. They showed that only the high-energy flux of non-thermal electrons drives explosive evaporation, accompanied by the formation of cool chromospheric condensations in the flare chromosphere.

Another situation occurs when the flux associated with non-thermal electrons is low. Then only a weak chromospheric evaporation takes place. This kind of evaporation is referred to as *gentle evaporation* (Antiochos & Sturrock 1978; Fisher et al. (1985b); Schmieder et al. 1987) and it can be observed in transition region lines and in chromospheric spectral lines like Hα or in Ca II (8542 Å). Antiochos & Sturrock suggested that the gentle chromospheric evaporation may occur after the primary energy release when the non-thermal electron flux has stopped. This evaporation could be driven by the large conductive heat flux from a high-temperature flare plasma contained in magnetic tubes above the chromosphere (Fisher et al. 1985b). Such physical conditions may appear during the gradual phase of solar flares, when there is no significant flux of non-thermal electrons. In the Forbes et al. (1989) model for flare-loop formation by magnetic reconnection the conduction of the thermal energy generated at the slow-mode shocks drives a gentle evaporative upflow from the ribbons.

Schmieder et al. (1987) observed small but long-lasting blue shifts in flare ribbons in the Hα line during the gradual phase of three solar flares and interpreted them as due to upflows with velocities $<$ 10 km s^{-1}. These upflows were thought to be caused by a gentle chromospheric evaporation driven by the heat conduction along the field lines connecting the chromosphere with a reconnection site in the corona. In the case of gentle evaporation, the observed

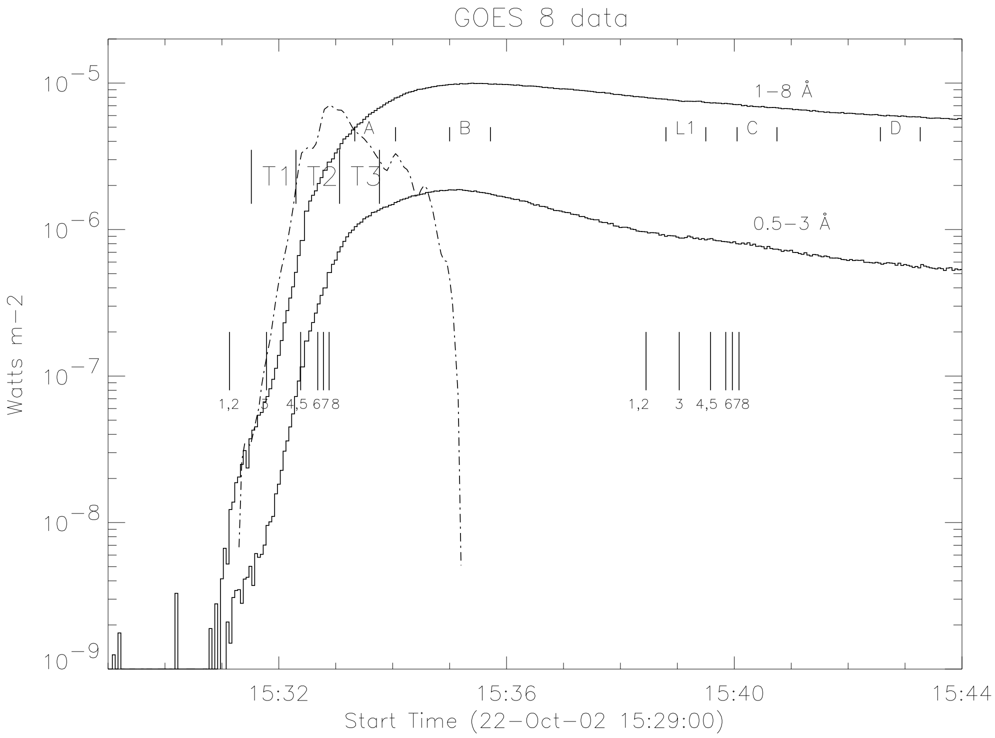

Fig. 1. Time evolution of the GOES 8 X-ray fluxes on October 22, 2002 during the M1 flare and the CDS raster scan. The dot-dashed curve is the time derivative of the 0.5–3 Å light curve, and can be used as a proxy for the hard X-ray emission. The timings of a few key observations are indicated (top: CDS slit positions, see Fig. 3; middle: TRACE images, see Fig. 4; bottom: Hα slit positions during two consecutive rasters, see Fig. 11).

flow velocities are much lower than during the impulsive phase of flares.

The analysis of gentle evaporation during the gradual phase using chromospheric lines is quite complex since the line profiles can be in absorption or enhanced emission. Very often we also observe self-reversed profiles. Deducing the velocity from such profiles is rather difficult and cannot be done just by searching for Doppler shifts with the bisector method (Heinzel et al. 1994). Chromospheric line profiles suggest that the flare atmosphere is highly dynamic and stratified with rather complicated plasma motions. In addition, these lines are optically thick. The most reliable way to analyse the velocity field is to use the non-LTE radiative transfer codes, which enable us to compute the chromospheric models with velocity fields. Resulting synthetic line profiles can then be compared with the observed ones. The analysis by Teriaca et al. (2003) is severely limited in this respect, since the velocities in the chromosphere were obtained soley from the relative shifts between Gaussian fitted profiles. This can lead to inaccurate results concerning the magnitude and even the direction of the chromospheric flows.

A coordinated observational campaign was organised to follow the evolution of the NOAA 0162 active region during October 22, 2002. Ground based instruments (THEMIS and Vacuum Tower Telescope - VTT - on Tenerife, Canary islands, Spain) and space observatories (SOHO, TRACE and RHESSI) were involved. The active region had several flares, including an M1 flare. The morphology and evolution of the M1 flare in particular during the gradual phase (when RHESSI was observing) were presented in Berlicki et al. (2004). Here, we focus in particular on the nature of the emission from the high temperature plasma, as seen in the initial phase of the M1 flare with the CDS on SOHO.

In this paper we focus primarily on the nature of the blue shifted emission from high temperature plasma and its relationship with the cool chromospheric emission and the hot flare emission. In Sect. 2 we summarise the observing campaign for the 22nd October 2002. In Sect. 3 we present the CDS observations and results in detail, paying particular attention to the measurement of wavelength shifts. In Sect. 4 we discuss the VTT Hα observations and the method used to derive chromospheric flows from the spectral line profiles. In Sect. 5 we draw our conclusions from these observations.

2. Co-ordinated observing campaign for 22nd October 2002

The active region NOAA 0162 was mainly bipolar, quite extended, and relatively active. It was observed on October 22, 2002 with SOHO, TRACE, RHESSI, and from the ground with THEMIS and VTT. The SOHO/CDS sequence of observations was extensive and ran during 08:02-13:07 UT and 15:18-18:13 UT (see

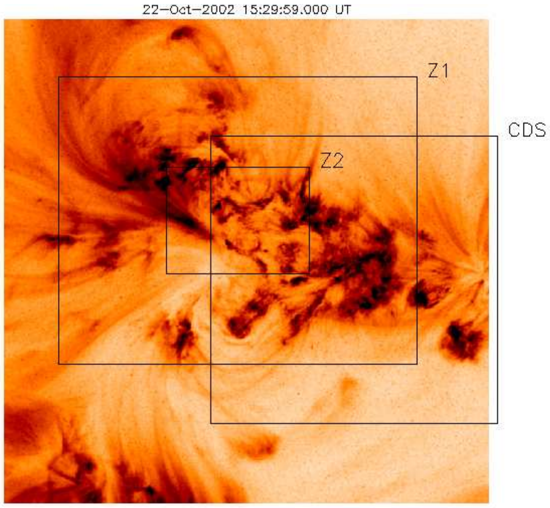

Fig. 2. TRACE 195 Å image of the active region before the M1 flare. The fields of view of the TRACE sequence of images (Z1, see Fig. 3), of the region of the M1 flare (Z2, see Fig.4), and of the CDS raster are also shown.

Table 1). The CDS observations, described in detail below, consisted of 'rasters' during which the slit was scanning the active region.

During October 22 the active region produced at least 3 flares, all of which were recorded by CDS. A relatively strong flare was recorded during the CDS raster at 12:43–13:07 UT. The second, main M1 flare is the focus of this paper. It occurred during the CDS raster at 15:18:16–15:43:16 UT. Fig. 1 shows the X-ray light curves from GOES 8 during the CDS scan. The time derivative of the 0.5–3 Å light curve can be used as a proxy for the hard X-ray emission, and indicates a peak at 15:33 UT. The timings of some CDS slit positions and some TRACE and ground-based observations are also shown.

Table 1. CDS rasters analysed - 22 Oct 2002.

Time (UT)	CDS files	CDS study
8:02:50–8:27:54	s26053r00	SIG_FT44
	s26054r00	ARDIAG_2
	s26054r01	ARDIAG_2
	s26055r00	ARDIAG_2
	s26056r00	SIG_FT44
15:18:16–15:43:16	s26058r00	SIG_FT44
15:43:30–17:07:33	s26059r00	ARDIAG_2
17:08:03–18:32:46	s26059r01	ARDIAG_2

A third flare, class C2, was recorded later by another CDS raster during 15:43:30–17:07:33 UT, and has been discussed in Berlicki et al. (2004). VTT/MSDP observations in Hα consisted of 9 raster scans between 15:30 and 16:17 UT and a field-of-view of about 380"×170" (exposure time of 0.5s). The rastering was performed from east to west, in the opposite direction compared to CDS. Below

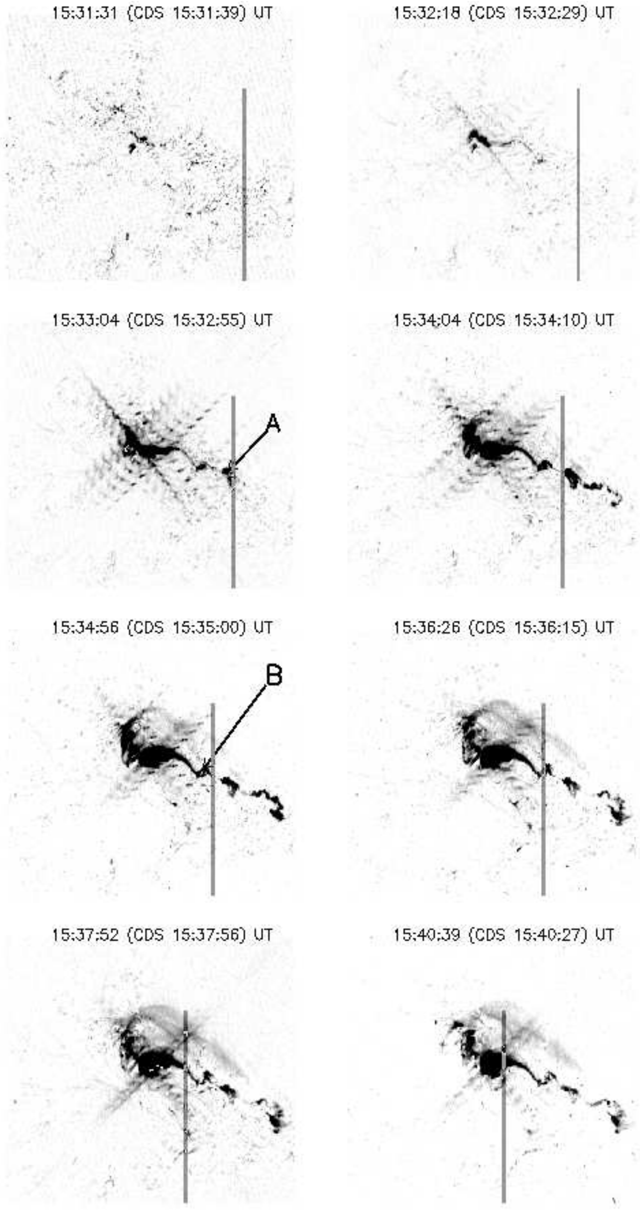

Fig. 3. Sequence of TRACE 195 Å difference images (negative) of the region Z1 (cf. Fig. 2) and centred during the peak of the M1 flare. The image that has been subtracted was taken at 15:29:59 UT, before the start of the flare. The timings indicate the initial exposure time for each TRACE image, and the corresponding nearest CDS exposure. The location of the CDS slit is also shown.

we will concentrate on the first VTT spectral raster, which scanned the active region during 15:30-15:37 UT, i.e. in the impulsive phase. Results from the follow-up raster (gradual phase) have been presented by Berlicky et al. (2005).

TRACE 195 Å images were obtained at high-cadence (40 s) between 15:29 and 15:41 UT (with a FOV 384"×384" and a 1" resolution). Before and after this time the TRACE observations were obtained with slightly lower time resolution (50 s) and larger FOV (512"×512"). Before the M1 flare, the active region presented the usual

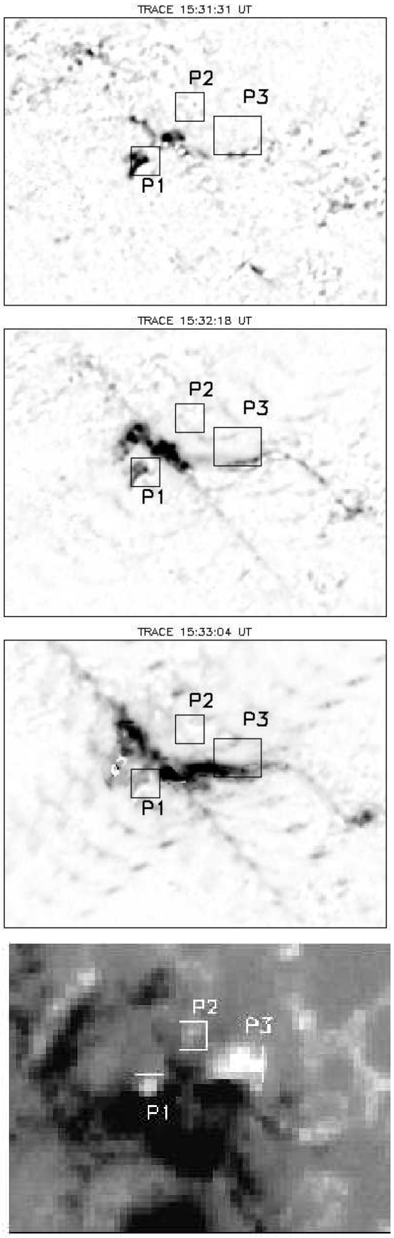

Fig. 4. Top: sequence of three (T1,T2,T3) TRACE 195 Å difference images (negative) in the region Z2 (cf. Fig. 2) of the M1 flare. Bottom: magnetogram from SOHO/MDI. The reference pre-flare image was taken at 15:29:59 UT. The areas P1, P2, P3 and their surrounding mixed-polarity regions experienced changes during the flare.

characteristics, as shown by the TRACE 195 Å images (see Fig. 2 for the full TRACE FOV). That is the active region consisted of some unresolved emission and a large number of loops.

Fig. 3 shows a sequence of TRACE 195 Å difference images in the central part of the TRACE FOV, where the flare took place. The location and timings of the CDS slit are also indicated in Fig. 3. The first obvious signature in the TRACE 195 Å occurs at 15:32:18 UT, somewhat later than the increase in the GOES X-ray flux. However, a small brightening already appears at the same location on the 15:31:31 UT TRACE image. The position of the flare and its relation to the underlying photospheric magnetic field is shown in Fig. 4, where a zoom-up of the same region is presented.

By 15:33 UT, the entire ribbon structures (located on either side of the neutral line) brighten up in the TRACE 195 Å image. The Hα ribbons were already visible at 15:31 UT (see Berlicki et al. 2004). The two emissions appear co-spatial. It is possible that the TRACE 195 Å emission in the brightest region consisted of a system of low-lying loops that connected the two polarities. At the same time, a fainter system of loops forms and expands in height, as shown in Fig. 3. These loops are rooted in the ribbons at specific points in the two opposite polarities. The interpretation of the structures seen in the TRACE 195 Å images is non-trivial, since the 195 Å band is mainly formed by the superposition of continuum emission and line emission from Fe VIII, Fe XII and Fe XXIV, all of which are formed at very different temperatures.

CDS had the slit positioned over the main area of the flare during the peak and gradual phase (cf. Fig. 1 and Fig. 3) and can therefore be used to estimate the temperatures of the various features recorded by TRACE. As shown below, CDS observed strong Fe XIX emission in the locations of both the ribbons and the higher-lying loops observed by TRACE, which suggests that most likely the TRACE images are dominated by hot emission from Fe XXIV.

SOHO/MDI took high-cadence (1m) full-disk magnetograms and dopplergrams during the observations of this active region. The flare was located above a region of strong mixed polarity, in particular in the middle of the unipolar areas P1, P2, P3 indicated in Fig. 4. The magnetograms do not show any dramatic changes during the flare. However, the three unipolar regions did experience measurable changes at the same time and positions in the flare as seen by TRACE. The magnetic fragment P1 (of the leading polarity), embedded in a region of opposite polarity, is the first one to show (at 15:31 UT) a drop of 100 gauss The entire surrounding area subsequently develops changes (indicating some flux cancellation). Unfortunately most variations appear to occur on small spatial scales and are at the limit of the sensitivity of the instrument (20-30 gauss). Furthermore, the measured values are time-averaged line-of-sight components, and it is therefore difficult to attempt a detailed reconstruction of the topology of the magnetic field and its variations.

3. CDS instrument and data analysis

The CDS observations were performed with the normal incidence spectrometer (NIS). The internal scan mirror allows CDS to scan an area of $4'$ square within a single 'raster', from west to east. The N-S coverage was provided by the use of the long slit $4''$x$240''$.

The NIS is composed of two gratings, that produce two wave-bands (NIS 1: 308 – 379 Å and NIS 2: 513 – 633 Å;). Telemetry constraints made it necessary to pre-select

Table 3. Some of the prominent lines in the CDS/NIS wavelength bands, used in this paper. Wavelengths are taken from the CHIANTI database unless otherwise stated. Those indicated with an asterisk have been used for the wavelength calibration. When only one decimal place is indicated, the lines are blends of at least two transitions. The approximate temperature of maximum ion abundance (in ionization equilibrium) is also indicated, together with the channel and the CDS study that recorded the lines (FR: fast raster; DR: diagnostic raster, see text).

Ion	wavelength (Å)	log T_e	NIS	
Fe XIV	334.172	6.2	1	DR
Si X	347.402	6.1	1	FR,DR
Si X	356.0	6.1	1	FR,DR
Fe XVI	360.761	6.3	1	DR
Fe XII	364.467	6.1	1	DR
Mg VII	367.7	5.8	1	DR
Mg IX	368.070	6.0	1	DR
Si XII	520.665*	6.3	2	FR,DR
He I	522.210*	4.5	2	FR,DR
Ne IV	542.07*	5.3	2	DR
Al XI	550.06*	6.2	2	DR
O IV	553.34*	5.3	2	FR,DR
O IV	554.076	5.3	2	FR,DR
O IV	554.513	5.3	2	FR,DR
O IV	555.263*	5.3	2	FR,DR
Ca X	557.765*	5.8	2	DR
Ne VI	558.594*	5.6	2	DR
Ne VII	561.728	5.7	2	DR
Ne VI	562.803*	5.6	2	DR
Fe XIX	592.16	6.9	2	FR,DR
Fe XII	592.60*	6.1	2	FR,DR
Mg X	624.941*	6.0	2	FR,DR
O IV	625.853	5.3	2	FR,DR
O V	629.732*	5.4	2	FR,DR

a number of NIS wavelength windows to be extracted onboard from the spectra, before the data are telemetered to the ground.

The CDS observing sequences were specifically designed to study the spatial and spectral characteristics of small flares. They included a range of spectral lines from different ions and in particular the high temperature flare line, Fe XIX 592.2 Å. CDS observed NOAA 0162 with the two types of rasters (see Table 1): 1) a slow diagnostic raster (1hour 20 m, CDS study name ARDIAG_2) that extracts many diagnostic lines; 2) a fast raster (slit exposure of 18s for a total duration of 20 m, CDS study name SIG_FT44) that only extracts a few lines, selected to cover a wide range of temperatures (see Table 3).

One important aspect of CDS is that lines emitted from the chromosphere up to the corona are observed. This is very useful for a proper co-alignment with other datasets, e.g. photospheric magnetic fields from SOHO/MDI, and coronal images from TRACE. A series of standard corrections was applied to the raw NIS data. These include de-biasing, flat-fielding, corrections for the burn-in of the lines and high count rates, cosmic ray removal. Multiple-line-fitting techniques have been used to determine the moments of each of the spectral lines in the spectra by removing the *'continuum'* intensity, which is mainly due to scattered light in the NIS. In SOHO post-recovery spectra, the CDS/NIS line profiles are no longer gaussians, and show a broadened and asymmetrical long wavelength wing, which is approximately constant and can therefore be accounted for. The CDS calibration of Del Zanna et al. (2001) has been adopted here, with a correction to take into account the effects on the NIS detector of the gain depression caused by exposures with the wide slit.

3.1. Wavelength calibration

For a correct interpretation of the velocities observed, an accurate wavelength calibration is necessary. CDS does not have an absolute wavelength calibration. Changes in the wavelength calibration have been observed (up to 0.1 Å in NIS 2), and caused primarily by on-board temperature changes (and their history), which are due to the variable illumination received from the Sun (D. Pike, priv. comm.). Also, the wavelength calibration often requires a 'scan mirror correction', which also appears to vary. In addition, there are no photospheric or chromospheric lines within the CDS wavelength bands (except He I).

The above means that the calibration has to be done using the observed transition region and coronal lines, and that it is necessary to obtain/check the wavelength calibration for each set of observations. We note, however, that in the literature it is standard practice (see, e.g. Brosius & Phillips 2004) to only make relative wavelength measurements, by using as reference values those obtained within the same set of observations, and without performing a wavelength calibration.

For the calibration, it is important to have accurate 'standard' rest wavelengths for the spectral lines concerned, which is a non-trivial issue if very accurate measurements are sought. We have adopted the values shown in Table 3. For most lines we adopt the wavelengths as in the CHIANTI database, which in turn has values mostly from NIST. We note, however, that the values in NIST are taken from the literature, where many measurements have been obtained from solar spectra. A simple survey in the literature shows that for most spectral lines wavelength measurements are inconsistent (i.e. differences are larger than the uncertainties in the measurements). These issues are discussed in a series of papers where atomic data (including wavelengths) are benchmarked on an ion-by-ion basis (cf. Del Zanna et al. 2004)

The case of the important Fe XIX 592.2Å line is emblematic. A large number of different measurements can be found in the literature. Our calibration, based on a small sample, provides a wavelength of 592.16 Å, in excellent agreement with the accurate measurements of Widing (1978), but different from e.g. the value previously re-

Table 2. List of the main lines used for the wavelength calibration. The first row gives the reference wavelengths (λ_{st}, Å) adopted. The second row gives the wavelengths (λ_1, Å) as obtained from the pre-flare raster s26055 and the calibration curve adopted. The third row gives the corresponding relative velocities (v_1, km/s). The following two rows give wavelengths (λ_2, Å) and relative velocities (v_2, km/s) as obtained from the post-flare raster s26059 and using the same calibration curve. Note the small differences in the measured wavelengths, giving confidence in the stability of the wavelength calibration.

	Si XII	He I	Ne IV	Al XI	O IV	O IV	Ca X	Ne VI	Ne VI	Fe XII	Mg X	O V
λ_{st}	520.665	522.210	542.07	550.06	553.34	555.263	557.765	558.594	562.803	592.60	624.941	629.732
λ_1	520.675	522.208	542.031	550.070	553.365	555.252	557.758	558.590	562.791	592.590	624.936	629.735
v_1	5	-1	-21	5	13	-6	-3	-2	-6	-5	-2	1
λ_2	520.664	522.211	542.061	550.066	553.354	555.260	557.769	558.622	562.812	592.597	624.932	629.747
v_2	0	0	-4	3	7	-1	1	15	5	-1	-4	6

ported by Sandlin et al. (1976), 592.24 Å. We note that Widing (1978) averaged many flare observations taken with the NRL spectroheliogram on Skylab. On the other hand, Lawson & Peacock (1980), in their review of the $n = 2 \rightarrow n = 2$ transitions, based on solar and laboratory measurements, suggested an energy for the $2s^2\ 2p^4\ ^1D_2$ level of 168770 cm^{-1}. This energy is equivalent to a rest wavelength of 592.522 Å, i.e. at the considerable difference of 183 km/s, compared to our result, 592.16 Å. An extra complication is due to the presence, in the red wing of the Fe XIX line, of a coronal line only recently identified as due to Fe XII (see Fig. 9 below and Del Zanna et al. 2002a, Del Zanna & Mason 2004).

To calibrate the CDS observations, average CDS spectra containing a large number of lines (the diagnostic rasters) of two rasters taken before and after the flare have been analysed and wavelength-calibrated. We assumed for the CDS pixel-wavelength calibration a quadratic function. The wavelength calibration was remarkably stable over the period. Table 2 shows that in most cases the line centres were within a few km/s the assumed reference values.

In terms of uncertainties, we note that the positions of the line centres can be calculated with approximately 1/10 of a pixel accuracy (1 pixel in the NIS 2 channel is approximately equivalent to 0.11 Å), and the average differences between the predicted and standard wavelengths are of the same order, 0.01 Å. This accuracy results in an uncertainty in the derivation of velocities of the order of 10 km/s. An additional systematic uncertainty is due to the spatially-dependent effects due to the geometrical distortions within the instrument. This is more difficult to quantify, because it depends on the type of relative measurement that is done, but is again of the same order. Finally, we note that the resolution of the CDS instrument does not allow simultaneous measurements of stationary and non-stationary components. Hence, our results refer in most cases to the average main displacement of each line profile. This is not true in the case of the Fe XIX emission, since it is present only during flares. Signicant line broadening can however be measured even in post-recovery spectra.

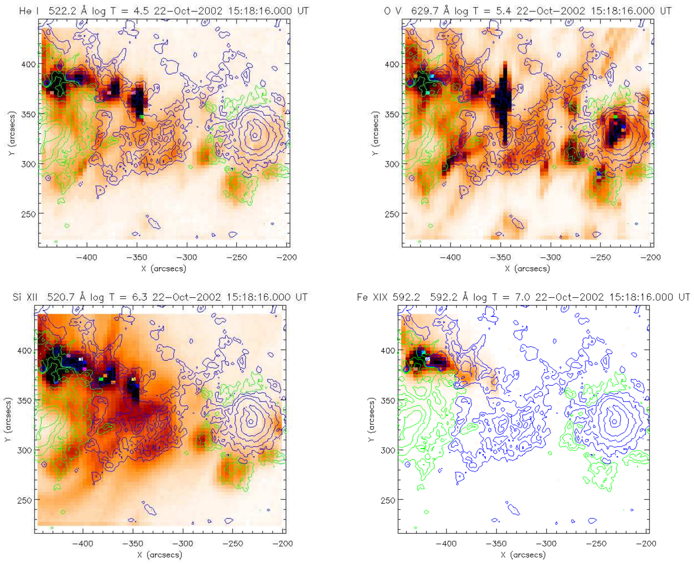

Fig. 5. Monochromatic images obtained from the CDS raster. Contours from the SOHO/MDI magnetograms are superimposed.

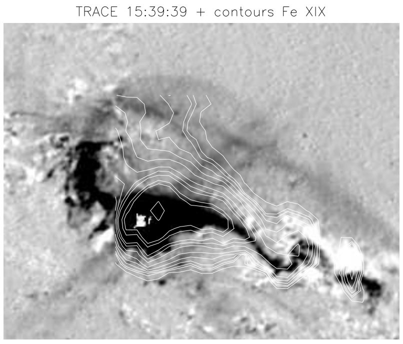

Fig. 6. TRACE 195 Å difference (negative) image with contours of Fe XIX intensity.

3.2. Overview of the CDS results

Fig. 5 shows monochromatic images obtained from the CDS raster, in lines emitted over a broad temperature

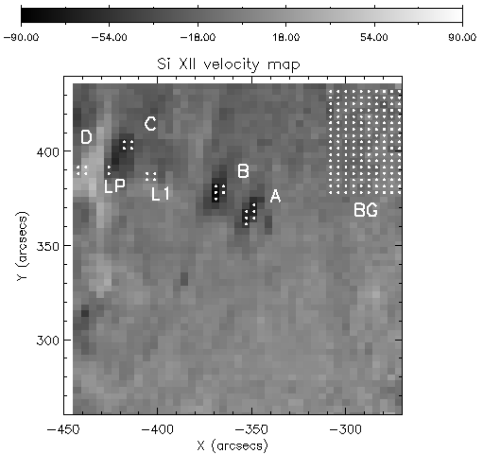

Fig. 7. Si XII λ520.665 Å velocity map in the flare region, with the areas selected for further analysis. Areas A,B,C correspond to regions of strong blue-shifts, while area D of red-shift. Region LP corresponds to the area of peak Fe XIX λ592.16 Å intensity, while region L1 is where the central part of the flare loop is located. Region BG is a 'background' reference region.

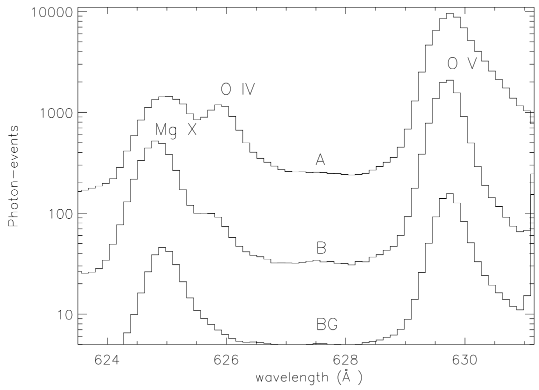

Fig. 8. Spectra of three different regions, A,B,BG. Note that in region A the profiles of the strongest lines are nearly saturated. The O IV line has been used for density measurements at transition-region temperatures.

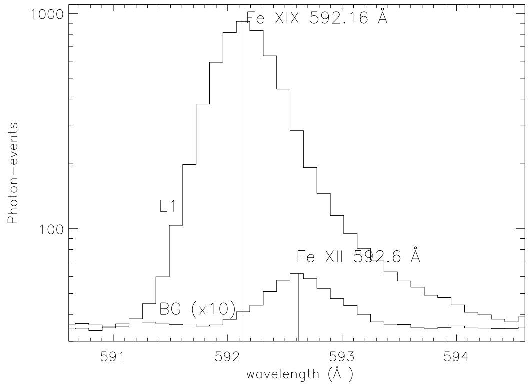

Fig. 9. Spectra of the region L1 (peak flare), and of the background BG (multiplied by ten), showing the Fe XIX λ592.16 Å and the previously unidentified Fe XII line. Outside of the flaring region, all the intensity is due to Fe XII.

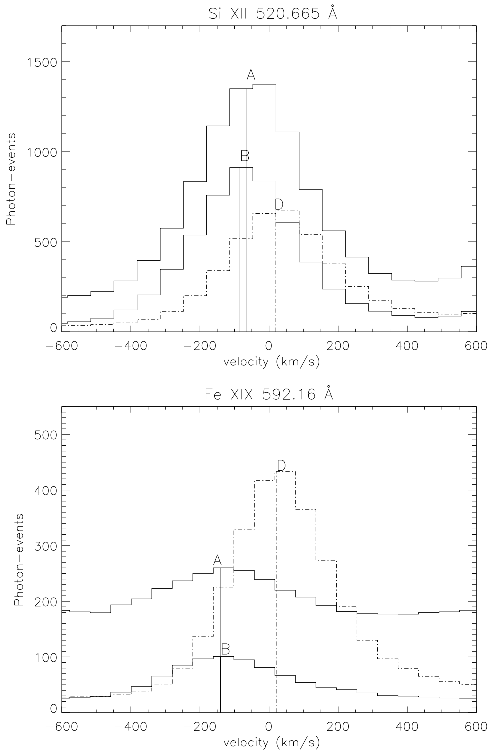

Fig. 10. Line profiles in regions A,B,D showing the evident blue-shifts in the coronal (Si XII) and flare (Fe XIX) lines in regions A,B.

range. The ribbon structure is so bright in He I and also at transition region temperatures (e.g. O V) that the brightest lines saturated the detector in some positions (region A, defined below). The hot emission from Fe XIX is only present in the ribbon and high-lying loop structures seen in the TRACE 195 Å band (see Fig. 6).

The velocity maps show a consistent pattern. Large velocities, mainly upflows, are only visible in lines formed above 1 MK, and in the Fe XIX flare line. Fig. 7 (top) shows as an example a velocity map in the flare area obtained from a Si XII line, and the regions selected for further study. Line fitting was performed on the averaged spectra of these selected regions. Figs. 8,9,10 show some line profiles in a few selected regions. Table 4 presents some results of the line fitting, in particular velocities, intensities and line widths.

Regions A,B were associated with the brightest emission in the chromospheric-TR lines, and with strong upflows in the Fe XIX flare line. Region A was observed by CDS during 15:33:20–15:34:10 UT (see Fig. 3 for the correspondence with TRACE), i.e. in the impulsive phase of the flare (Fig. 1). Region B was observed during 15:35:00–15:35:50 UT, i.e. at the time of the peak X-ray emission (Fig. 1).

As observed in other cases (Del Zanna et al. 2002b), upflows are also seen in the lower-temperature Si XII and Mg X lines. Our findings are contrary to those of Brosius & Phillips (2004), that discouraged the use of Mg X lines because of blends with O IV emission.

In terms of line widths, aside from a few notable exceptions, the full-width at half maximum ($FWHM$) values are close to the value of the instrumental width (0.5 Å in post-recovery spectra). The exceptions are in regions A,B,D and mostly in the coronal lines. Interestingly, the Fe XIX line has a large width in all of the regions, suggestive of large turbulent motions. As also noted by Brosius & Phillips (2004), the observed blue-shifts are not superimposed on a stationary component, but appear as shifts of the entire line profiles in Mg X, Si XII and Fe XIX (see Fig.10).

We also find upflows (although smaller) in the TR lines in region B. Interestingly, in region A, during the impulsive phase, He I, O IV and O V lines show small downflows. However, these results should be considered with some caution because the detectors were nearly saturated (completely saturated in the O V case).

The other regions were close to the flare site. Region L1 shows near-zero line-of-sight velocities in all lines. The region LP corresponds to the area of peak X-ray emission, as judged from the TRACE 195 Å images and the Fe XIX emission, observed by CDS 7 minutes later, around 15:42 UT. It is interesting to notice that, on the opposite sides of the peak emission, flows of opposite directions are observed (region C, upflow; region D, downflow) in all the lines, emitted from TR to flare temperatures.

Region BG was chosen as a background reference region, not interested by the flare. The lines show near-zero line-of-sight velocities. Note that the intensity of the Fe XIX line is an upper limit (the emission being dominated by the Fe XII). We have compared the line intensities of the background region with other observations of the quiet Sun, and found that, for the transition region lines, the values are very close to those of the average quiet Sun.

The O IV lines (cf. Fig. 8) are an useful density diagnostic at transition region temperatures, and in the locations of strong brightenings. For both the upflow regions A and B we obtain averaged line-of sight electron densities of $\simeq 10^{11}$ cm^{-3}. Interestingly, the O IV intensities increase by factors of $\simeq$300, 20, while the density increases by an order of magnitude compared to quiet Sun values (cf. Del Zanna & Bromage 1999). This means that the filling factor of the two regions could be different. This is an added complexity that a detailed flare interpretation should take into account.

4. Hα line profiles

For the analysis of the Hα Dopplershifts we used the observations of VTT/MSDP obtained at 15:30-15:36 UT. We selected areas (Fig. 11) corresponding to the regions observed by SOHO/CDS (see Fig. 12). Regions 6,7,8 in the Hα spectra correspond to region A in the CDS spectra; 4,5 to region B; and 3 to region L1.

The mean profile of Hα line from each analysed area was obtained by averaging the spectra from nine pixels contained inside a square box $0.75 \times 0.75''$, the distance between two neighbouring pixels being equal to $0.25''$. We used these profiles to derive the velocity structure of the flaring chromosphere in the eight respective bright kernels. Fig. 13 presents these averaged profiles (continuous lines). These profiles are typical for flares, which often have double-peaked emission with a central reversal. All observed profiles are asymmetrical, indicating the presence of vertical motions in the chromosphere.

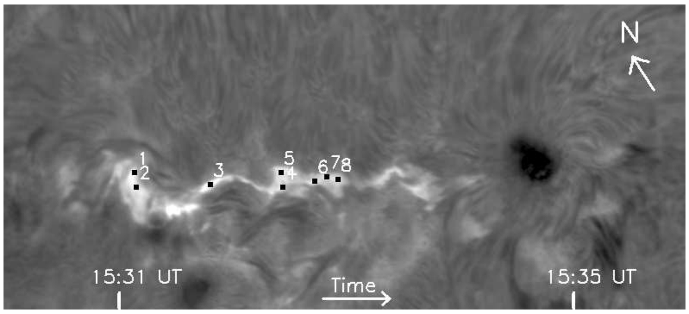

Fig. 11. VTT/MSDP image of AR 0162 taken between 15:30 and 15:36 UT with dots which mark the areas where the Hα line profiles were obtained. The timing and scanning direction are also indicated.

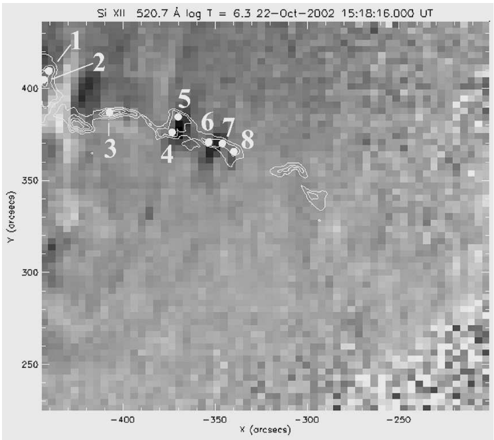

Fig. 12. SOHO/CDS velocity map in the Si XII 520.7 Å line obtained between 15:18 and 15:43 UT. The darker structures represent upflows. The dots (1-8) mark the areas where the Hα line profiles were obtained The contours represent the Hα flare ribbons as observed by VTT during 15:30-15:36 UT.

In order to construct the models of the solar chromosphere corresponding to the analysed areas of the flare, we follow the method discussed in Berlicki & Heinzel (2004), which consists of two steps. First, a grid of static models is calculated with the non-LTE code developed by Heinzel (1995), and modified for flare conditions (Berlicki & Heinzel 2004), by varying two parameters m_0 and ΔT. A least-square fit is then applied to the observed and synthetic Hα line profiles. The m_0 and ΔT values obtained are given in Table 5 (second and third columns).

Table 4. Results from the averaged spectra of the various regions displayed in Fig. 7. For each of the selected spectral lines, we display the averaged velocities v (in km/s; negative corresponds to blue-shift), the calibrated line intensities I (erg cm^{-2} s^{-1} sr^{-1}), and the full-width at half maximum $FWHM$ (Å). O IV(a) indicates the 553.4 Å line, while O IV(b) indicates the 625.8 Å line, used to obtain the electron densities N_e (cm^{-3}). Large blue-shifts are mostly observed in regions A,B,C. Note, however, that some of the lines are close to saturation in region A, and values are uncertain (they are indicated in parentheses).

Region	A	B	C	D	L1	LP	BG
He I v	13	-27	-30	-17	-17	-36	-22
I	2393	770	112	377	751	1293	16
$FWHM$	0.61	0.53	0.51	0.56	0.51	0.51	0.50
O IV(a) v	(33)	-21	-24	13	0	-20	0
I	(9818)	598	80	237	252	686	33
O IV(b) I	2333	111	-	-	-	-	-
N_e (O IV)	2 10^{11}	0.9 10^{11}	-	-	-	-	-
O V v	(23)	-25	-21	0	-12	-28	-4
I	(33226)	5038	721	2490	2840	6782	387
$FWHM$	(0.70)	0.50	0.50	0.55	0.50	0.50	0.50
Mg X v	(14)	-62	-51	29	-17	-37	-5
I	(5910)	1630	656	1205	1781	17093	118
$FWHM$	(0.80)	0.59	0.53	0.58	0.58	0.52	0.52
Si XII v	-64	-84	-54	17	-6	-40	-10
I	2756	1847	839	1378	2818	16748	63
$FWHM$	0.59	0.55	0.50	0.55	0.51	0.50	0.50
Fe XIX v	-141	-140	-56	22	-13	-26	-
I	294	272	694	1271	2721	7544	≤ 0.5
$FWHM$	0.68	0.65	0.56	0.59	0.57	0.55	-

Second, to investigate the influence of the macroscopic velocity field on the emergent Hα line profiles we adopted the formula used by Mihalas (1978) to describe an expanding atmosphere. This formula was previously used in the modelling of the velocity field in flaring atmosphere by Nejezchleba (1998) and Berlicki et al. (2005). The vertical velocity as a function of the Hα line-centre optical depth was defined as:

$$V(\tau) = \frac{2V_0}{1 + \tau/\tau_m}. \qquad (1)$$

τ_m corresponds to the height where the velocity is equal to V_0. If $\tau \ll \tau_m$, which corresponds to upper layers of the chromosphere, the velocity goes to $2V_0$, and for $\tau \gg \tau_m$ (close to the photosphere) the velocity reaches zero. As was shown by Berlicki et al. (2004) such a vertical structure of the velocity field seems to be a reasonable representation of an evaporating atmosphere. A second grid of synthetic Hα line profiles was computed using different values of V_0 and τ_m, and a best-fit with each observed profile performed. The fitted profiles are shown in Fig. 13. The parameters describing the velocity field in the various areas are also given in Table 5 (forth and fifth columns). The vertical velocity parameter V_0 was corrected with the value of direction cosine $\mu = 0.8$ assuming that the velocity vector is perpendicular to the solar surface. Negative values of V_0 parameter means upward flows.

4.1. Models of the flaring chromosphere

Table 5. The parameters m_0 and ΔT of the static models and log τ_m and the vertical velocity V_0 of the models with velocity obtained from the fitting of synthetic Hα line profiles with observed ones. The negative sign of the velocity means upflow.

Area	m_0[g cm^{-2}]	ΔT[K]	log τ_m	V_0[km s^{-1}]
1	$1.0 \cdot 10^{-3}$	+100	−0.4	downflow (?)
2	$1.0 \cdot 10^{-3}$	−200	−0.2	downflow (?)
3	$1.0 \cdot 10^{-3}$	+50	+0.4	+10.0
4	$8.0 \cdot 10^{-4}$	−100	+1.0	−1.9
5	$8.5 \cdot 10^{-4}$	−200	+0.1	−3.8
6	$8.5 \cdot 10^{-4}$	−250	−0.8	−9.4
7	$9.5 \cdot 10^{-4}$	−300	−0.1	−5.6
8	$1.0 \cdot 10^{-3}$	−400	0.0	−6.9

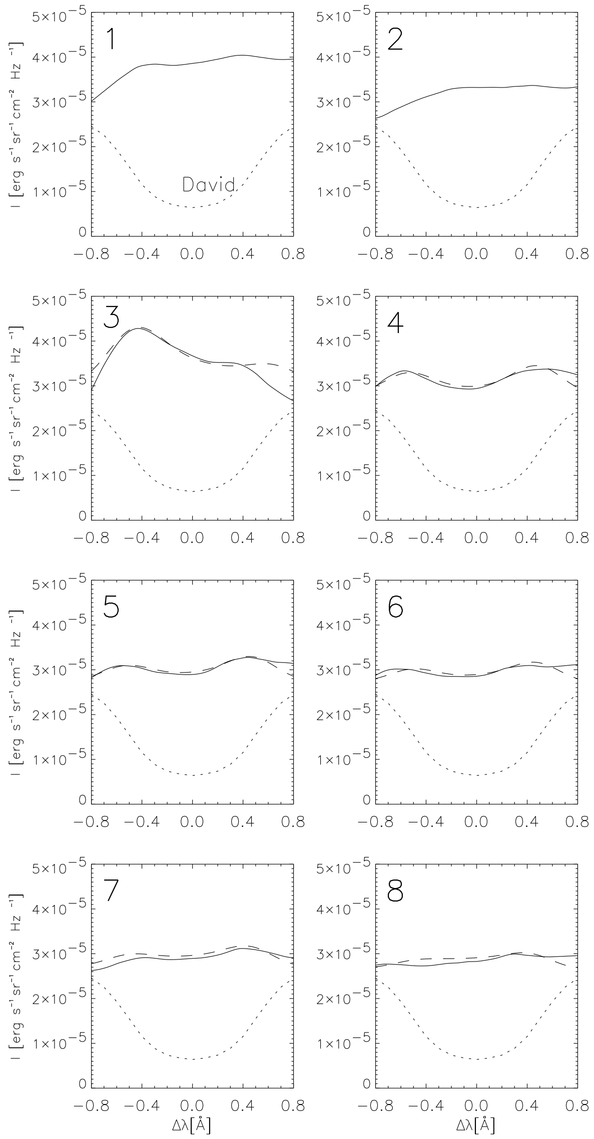

Fig. 13. The observed (continuous lines) and fitted (dashed lines) Hα line profiles in areas No. 1 - 8 of the flare. With dotted line we also plotted the mean profile of the quiet-Sun chromosphere taken from David (1961) for $\mu = 0.8$. For areas 1 and 2 we did not show fitted profiles (see text).

Most of the profiles in the flare ribbon areas exhibit a red asymmetry manifested by the slight increase of the intensity in the red wing around $0.4 - 0.5$ Å. In the case of self-reversed profiles the red asymmetry means an upflow. Among the eight analysed line profiles, one of them indicated downflow velocity and in five line profiles we found upward flows (see Table **??**). Interestingly, the same analysis performed on the following raster by Berlicki et al. (2005) indicates very similar upflows, which suggests that they were a long-lasting feature.

Fig. 14 shows the blue-shifts in region B observed by CDS, together with the corresponding value obtained from the Hα measuerements.

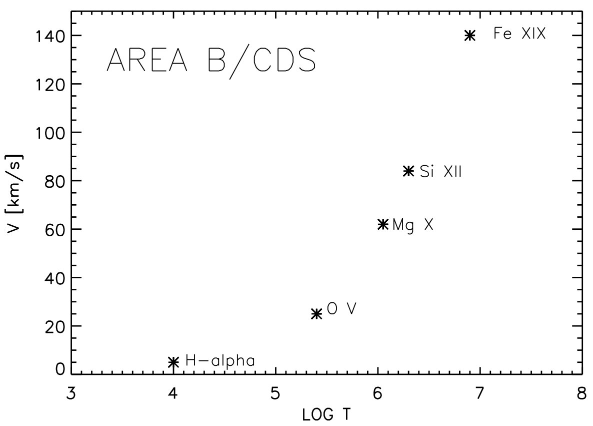

Fig. 14. Observed blue-shifts in region B

The profiles in areas 1 and 2 are very flat or asymmetric and cannot be fitted with satisfactory quality. The shape is consistent with strong downflows.

The non-LTE codes allows us also to calculate the electron densities at different heights of our model atmospheres. The models of solar atmosphere contain the layers from the photosphere to the chromosphere-corona transition region (CCTR). The CCTR temperatures obtained for the analysed areas 1-8 are $\simeq 10^5$ K. The electron densities N_e are $\simeq 1.0 \cdot 10^{12}$ cm^{-3}.

5. Discussion and conclusions

Some interesting aspects of the flare have been observed and deserve further comment.

The co-spatiality between the CDS Fe XIX and the TRACE 195 Å emissions suggests that the bulk of the TRACE 195 Å emission at the flare site is due to Fe XXIV. The TRACE 195 Å images, together with the SOHO/MDI magnetograms, clearly indicate that the location of the peak X-ray emission recorded by GOES is above a region of strong mixed polarity. Imaging in a flare line at high-time resolution (< 1m) is obviously a requirement for future observations.

Interestingly, in the same region the MDI magnetograms show small (at the limit of the sensitivity) but significant changes, co-temporal with the TRACE/GOES light curves. The changes occur on short time-scales (minutes) and indicate permanent flux cancellation in the area of highly-mixed polarities. There is a large body of literature on ground-based and space magnetic field observations before/during/after a flare. The results are controversial in the sense that changes in the magnetic fields have only been observed in a few cases. Small variations based on MDI magnetograms, but on longer timescales and on much larger flares have been reported (cf. Kosovichev & Zharkova 2001). It is therefore quite surprising to see measurable changes on timescales of one minute for a relatively small flare.

However, for a global interpretation of the event, one should keep in mind that the MDI measurements only provide an estimate of the line-of-sight component of the magnetic field. Furthermore, some doubts have been expressed about the MDI measurements themselves. For example, accelerated particles and radiation can alter the continuum and the profile of the lines used to infer magnetic fields, with the effect that the standard methods can provide incorrect values for the magnetic fields (see, e.g. Ding et al. 2002 for a discussion on MDI magnetograms). A correct interpretation would require full line profile and continuum measurements and a non-LTE model which would take into account of all processes that can affect the formation of the observed line from which the magnetograms are obtained. Future instruments such as those on SOLAR-B will have a much higher sensitivity and will produce vector magnetographs, which will greatly enhance our understanding.

CDS has measured flows in this flare in spectral lines formed over a range of temperatures (log T=5.4-6.9) with an accuracy $\simeq$10 km/s. As seen in our observations of many other small flares, we find upflows in 'hot' lines that are concentrated in small spatial areas, at the footpoints of coronal/flare loops. Stronger upflows are in the Fe XIX line, indicating that (as we already knew) most of the action takes place in the hotter lines. The large broadenings of the Fe XIX line are in fact indicative of the presence of turbulent motions, in addition to the overall flows.

Coronal images alone give no indications whatsoever on where flows could be located. The strongest flows seem to be observed in regions of low emission. Spectral observations of flare lines at high-time resolutions are needed. SOLAR-B EIS will have such capabilities.

There seems to be no clear one-to-one correspondence between the TR brightenings and the flows observed in the coronal emission. Fast imaging in TR lines would be useful, considering that most of the radiative losses occur in the transition region. Spectral observations with high resolutions would be needed to measure filling factors. Unfortunately, no planned instrument will have such capabilities.

An important diagnostic tool available with spectroscopic instruments is the possibility of measuring electron densities over a range of temperatures. We were able to use the CDS O IV diagnostic lines to obtain electron densities of the order of 10^{11} cm^{-3} for the regions A,B. These are somewhat lower that the values of 10^{12} cm^{-3} derived from the Hα data.

The Doppler-shifts of the chromospheric ribbons (10^4 K) have been derived from the profiles of Hα using a non-LTE radiative transfer code with a flare model and a velocity function (Berlicki et al. 2005). To our knowledge, this is only the second time (after Teriaca et al. 2003) that simultaneous and co-spatial chromospheric and coronal spectroscopic observations showing line shifts during flare are reported. In the C2 eruptive flare studied by Teriaca et al. (2003) upflows in coronal/flare lines corresponded to downflows in the chromosphere as seen in the He I 10830 Å line. In our case we have a different picture.

The enhanced intensity of the red wing observed for the Hα line profiles in areas 1 and 2 suggests that in these areas we observe large redshifts. These Hα line profiles were observed at 15:31 UT. This time corresponds to the increase of the GOES soft X-ray flux, which reached the maximum at around 15:35 UT. This suggests that these Hα profiles were observed during the impulsive phase. Such a type of asymmetry of Hα line profiles was reported in Ichimoto & Kurokawa (1984) and it can be caused by downward motion of the flaring chromosphere with velocities more than 40 km s^{-1}. Fisher et al. (1985a) suggests that such a downflow of cool chromospheric flaring plasma (chromospheric condensations) is caused by the enhanced pressure produced in the region heated by non-thermal electrons accelerated in the corona during the impulsive phase of solar flares. The downflow observed in cool chromospheric Hα line can be a reaction on explosive evaporation of hot plasma frequently observed in X-ray lines.

The areas that were observed simultaneously by CDS (A,B) and in Hα (regions 5,6,7,8) during the peak X-ray emission presented blueshifts which could correspond to the 'gentle evaporation' of the chromospheric plasma. The blueshifts are of the order of $5-10$ km/s in Hα, 27 km/s in He I, $60-88$ km/s in Mg X, Si XII, and 140 km/s in Fe XIX in region B. Region A shows instead downflows in the cooler lines observed by CDS, but the velocities are questionable given the fact that the emission saturates in the CDS detectors.

The eastern parts of the ribbons (areas C, D, LP in the CDS image and 1, 2 in the Hα image) which are closest to the onset location of the flare are not observed at the same time, so a comparison of the velocities is problematic. For the Hα ribbons (region 3), we measure a strong downflow. This could correspond to the impulsive downflow frequently observed during the impulsive phase. But according to the timing, region 3 was observed at 15:34 UT (3 minutes after the start time of the flare). One possibility is that the flare was composed of more than one burst. Another possibility is the formation of a siphon flow inside a loop joining the two areas anchored in the two opposite polarities where the main flare occurs. This possibility is supported by the presence of opposite flows (areas C and D) as seen at 15:40-15:43 UT in the coronal lines. (in Si XII and Fe XIX -55 km/s and +20 km/s respectively). It is reasonable that the evaporation was more effective in one footpoint and a siphon flow started a few minutes after the flare. Spectral observations with higher spatial resolution than CDS are needed, to study these kind of compact flares.

During a coordinated observing campaign, a compact and short-duration M1.0 flare was observed from the ground and in space using spectrographs. In this paper and in the previous one (Berlicki et al. 2004), which discussed the overall morphology and the magnetic topology of the active region, we adopted a multi-wavelength approach, i.e. we gathered together all the observational information relevant for a detailed study of the flare.

Firm conclusions on the mechanisms that trigger the event and detailed flare modelling cannot be achieved, given the (relatively) low spatial and temporal resolution of the current instrumentation. For example, as seen in the X-rays (GOES), the flare started at 15:31 UT and reached peak emission in just 3-4 minutes, i.e. on times shorter than the rastering times of the spectroscopic instruments. The SOHO/CDS and the VTT/MSDP instruments do allow us to make detailed studies of e.g. the velocities in the ribbons over a wide range of temperatures (10^4 K to $8 \cdot 10^6$ K). However, due to the scanning method of the spectrographs, we were only able to obtain spectra from a portion of the ribbons at the peak of the X-ray emission, and from the central area of the flare during the decaying gradual phase. Nontheless we are able to make some accurate measurements of velocities over a range of temperatures, for which we have proposed an explanation.

Other authors (e.g. Brosius & Phillips 2004) have adopted a different observing approach, i.e. to fix the slit position and rely on the imaging instruments to study the morphology of an event. The slit was fortitously positioned right where the flare took place.

Our observing campaign and analysis emphasises the importance of combining chromospheric and coronal observations in order to understand the dynamics of a solar flare. It is also essential to use spectroscopic observations to obtain an unambiguous determination of the plasma properties. Even so, with this set of observations, we have only just glimsed the complexity of chromospheric evaporation. The main problem with scanning instruments like VTT/MSDP and CDS is to be in the right place at the right time! Neither the scanning approach or the sit-and-stare approach is entirely satisfactory. We look to future projects, such as SOLAR-B, which will enable us to study active regions and flares in much more detail through all layers of the solar atmosphere.

Acknowledgements. GDZ and HEM acknowledge support from PPARC.

This research was partially supported by the European Commission through the RTN programme ESMN (European Solar Magnetism Network, contract HPRN-CT-2002-00313). AB and BS are members of ESMN.

SOHO is a project of international collaboration between ESA and NASA. These observations were performed during a MEDOC campaign (JOP 157).

We acknowledge the use of the SURF, TRACE, SOHO online databases.

References

Antiochos, S. K. & Sturrock, P. A. 1978, ApJ, 220, 1137
Antonucci, E., Gabriel, A. H., Acton, L. W., et al. 1982, Sol. Phys., 78, 107
Antonucci, E., Gabriel, A. H., & Dennis, B. R. 1984, ApJ, 287, 917
Bentley, R. D., Doschek, G. A., Simnett, G. M., et al. 1994, ApJ, 421, L55
Berlicki, A. & Heinzel, P. 2004, A&A, 420, 319
Berlicki, A., Heinzel, P., Schmieder, B., Mein, P., & Mein, N. 2005, A&A, 430, 679
Berlicki, A., Schmieder, B., Vilmer, N., Aulanier, G., & Del Zanna, G. 2004, A&A, 423, 1119
Brosius, J. W. & Phillips, K. J. H. 2004, ApJ, 613, 580
Czaykowska, A., de Pontieu, B., Alexander, D., & Rank, G. 1999, ApJ, 521, L75
Del Zanna, G., Berrington, K. A., & Mason, H. E. 2004, A&A, 422, 731
Del Zanna, G. & Bromage, B. J. I. 1999, J. Geophys. Res., 104, 9753
Del Zanna, G., Bromage, B. J. I., Landi, E., & Landini, M. 2001, A&A, 379, 708
Del Zanna, G., Gibson, S. E., Mason, H. E., Pike, C. D., & Mandrini, C. H. 2002a, Advances in Space Research, 30, 551
Del Zanna, G. & Mason, H. E. 2004, A&A, in press
Del Zanna, G., Mason, H. E., & Foley, C. 2002b, in ESA SP-506: Solar Variability: From Core to Outer Frontiers, 585–588
Ding, M. D., Qiu, J., & Wang, H. 2002, ApJ, 576, L83
Doschek, G. A., Kreplin, R. W., & Feldman, U. 1979, ApJ, 233, L157
Fisher, G. H. 1987, ApJ, 317, 502
Fisher, G. H., Canfield, R. C., & McClymont, A. N. 1985a, ApJ, 289, 434
Fisher, G. H., Canfield, R. C., & McClymont, A. N. 1985b, ApJ, 289, 425
Fisher, G. H., Canfield, R. C., & McClymont, A. N. 1985c, ApJ, 289, 414
Forbes, T. G., Malherbe, J. M., & Priest, E. R. 1989, Sol. Phys., 120, 285
Gibson, S. E., Fletcher, L., Del Zanna, G., et al. 2002, ApJ, 574, 1021
Heinzel, P. 1995, A&A, 299, 563
Heinzel, P., Karlicky, M., Kotrc, P., & Svestka, Z. 1994, Sol. Phys., 152, 393
Ichimoto, K. & Kurokawa, H. 1984, Sol. Phys., 93, 105
Kosovichev, A. G. & Zharkova, V. V. 2001, ApJ, 550, L105
Lawson, K. D. & Peacock, N. J. 1980, Journal of Physics B Atomic Molecular Physics, 13, 3313
Mason, H. E., Shine, R. A., Gurman, J. B., & Harrison, R. A. 1986, ApJ, 309, 435
Mihalas, D. 1978, Stellar atmospheres /2nd edition/ (San Francisco, W. H. Freeman and Co., 1978. 650 p.)
Nejezchleba, T. 1998, A&AS, 127, 607
Sandlin, G. D., Brueckner, G. E., Scherrer, V. E., & Tousey, R. 1976, ApJ, 205, L47
Schmieder, B., Forbes, T. G., Malherbe, J. M., & Machado, M. E. 1987, ApJ, 317, 956
Schmieder, B., Malherbe, J. M., Simnett, G. M., Forbes, T. G., & Tandberg-Hanssen, E. 1990, ApJ, 356, 720
Svestka, Z. 1976, Geophysics and Astrophysics Monographs, 8
Teriaca, L., Falchi, A., Cauzzi, G., et al. 2003, ApJ, 588,

596
Warren, H. P. & Doschek, G. A. 2005, ApJ, 618, L157
Widing, K. G. 1978, ApJ, 222, 735
Zarro, D. M., Slater, G. L., & Freeland, S. L. 1988, ApJ, 333, L99